Geochemical Perspectives Letters

Activity coefficients of siderophile elements in Fe-Si liquids at high pressure

K. Righter[1*], R. Rowland II[2], S. Yang[3], M. Humayun[3]

OPEN ACCESS
doi: 10.7185/geochemlet.2034

Abstract

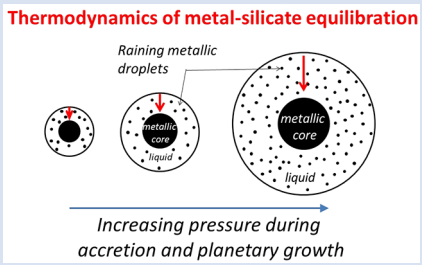

Metallic core formation in differentiated bodies in the inner solar system can take place between low pressures (near 1 bar) to much higher pressures (up to 100 GPa). Most thermodynamic models of metal-silicate equilibria utilise activity coefficients for metallic tracers in Fe liquids, nearly all of which have been carried out at low pressures. This study focuses on the effect of pressure on activity coefficients for Au, P, V, Mn, Ga, Zn, Cd, Sn, W, Pb, and Nb in liquid Fe-Si alloys. From a series of experiments at 10 GPa, 2373 K containing variable Si content in a metallic liquid we have derived epsilon interaction parameters in Fe-Si liquids (ε_M^{Si}). Comparison of 1 GPa and 10 GPa data shows no difference except for Nb. Epsilon parameters derived from low pressure experiments can thus be used to calculate activity coefficients for application to higher pressure processes (at least to 10 GPa).

Received 18 May 2020 | Accepted 10 September 2020 | Published 26 October 2020

Introduction

Light elements can alloy with Fe in the cores of terrestrial planetary bodies. Due to density considerations, Earth's core likely contains ~10 % of a light element, which could be a combination of S, C, Si, and O with Si probably being the most abundant (Hirose *et al.*, 2013). The dissolution of these elements, and in particular Si, is dependent upon oxygen fugacity (Righter *et al.*, 2020), which also controls the solubility of trace elements in metallic and silicate melts. Because Si is a major alloying agent in metallic cores, its solution in Fe metallic liquids can have a significant influence on the activity coefficients of siderophile elements, and thus the partitioning behaviour of those elements between the core and mantle (Tuff *et al.*, 2011; Righter *et al.*, 2018).

The Earth's core is estimated to have formed at pressures between 40–60 GPa (Wade and Wood, 2005; Righter, 2011; Siebert *et al.*, 2011). Pressure is known to influence volumetric properties of metallic and silicate liquids (*e.g.*, Armstrong *et al.*, 2019), and also affect oxygen fugacity (*e.g.*, Righter, 2016), but less is known about the effect of pressure on activity coefficients (*e.g.*, Steenstra *et al.*, 2020). If, for example, the activity coefficient of a moderately siderophile element (like W) in metallic Fe doubled, the corresponding concentration of that element in the silicate melt would nearly double as well. Thus even a modest change in activity coefficient will have a significant effect on mantle concentrations of siderophile element modelling outcomes. Understanding the effect of pressure on activity coefficients in the Fe-Si system, and in metallic liquids in general, is thus important for modelling core formation in the Earth and other terrestrial-like planets.

In this work, we carried out a series of experiments (See Supplementary Information Part 1, Fig. S-1, and Table 1) at 10 GPa to investigate the effect variable Si content has on the activity coefficients of Au, P, V, Mn, Ga, Zn, Cd, Sn, W, Pb, and Nb in Fe-Si alloys at 10 GPa and 2373 K. We derive interaction parameters for Fe-Si liquids for comparison to behaviour already investigated at 1 GPa, using the same starting materials (Righter *et al.*, 2018).

Results

Determination of epsilon interaction parameters. The epsilon interaction parameter (ε_M^{Si}) is a measure of the interaction between a trace element M and the solute Si in a Fe metallic liquid. The ε_M^{Si} approach for calculating activity coefficients allows effects of solutes like Si, S, and C to be quantified for a multicomponent metallic liquid (Supplementary Information Part 3). Positive ε_M^{Si} values indicate dissolved Si causes a decrease in partition coefficients, whereas negative values indicate an increase. Mn is the only element to exhibit a negative ε_M^{Si} of -1.1 ± 5.0 (standard error), and even this value is only marginally negative when error is considered. V and Zn have small, positive ε_M^{Si} of 3.5 ± 6.6 and 6.2 ± 3.3, respectively. Cd, Pb, Nb, and W all have positive but slightly lower ε_M^{Si} of 8.1 ± 1.3, 6.4 ± 1.8, 7.0 ± 8.3 and 14.3 ± 6.7, respectively (Figs. 1, S-2). Au, Ga, and Sn have moderate, positive ε_M^{Si} of 16.9 ± 3.7,

1. NASA Johnson Space Center, Mail Code XI2, Houston, TX 77058, USA
2. Los Alamos National Laboratory, Mail Stop P952, Los Alamos, NM 87545, USA
3. National High Magnetic Field Laboratory and Dept. of Earth, Ocean & Atmospheric Science, Florida State Univ., Tallahassee, FL 32310, USA
* Corresponding author (email: kevin.righter-1@nasa.gov)

Table 1 Silicate and metal compositions and partition and exchange coefficient summary (values in parentheses represent 2σ error).

Experiment	2	3	5	6	7
Silicate					
SiO_2	34.1(7)	37.4(7)	40.0(8)	41.0(8)	25.8(5)
TiO_2	2.14(2)	2.52(3)	2.58(3)	2.76(3)	1.27(1)
Al_2O_3	6.5(1)	8.2(2)	6.8(1)	9.4(2)	8.3(2)
FeO	3.00(3)	1.39(1)	0.170(2)	0.180(2)	0.070(1)
MnO	0.090(1)	0.060(1)	0.050(1)	0.040(1)	0.030(1)
MgO	42.1(8)	36.1(7)	38.0(8)	35.2(7)	54.6(1.1)
CaO	8.73(9)	10.63(11)	9.79(10)	9.05(9)	5.27(5)
Na_2O	1.15(2)	1.43(3)	1.76(4)	1.54(3)	1.05(2)
K_2O	1.04(1)	1.34(1)	1.60(2)	1.39(1)	0.75(1)
P_2O_5	0.060(3)	0.029(2)	0.024(2)	0.014(1)	0.016(1)
Total	98.87	99.04	100.75	100.54	97.19
Au (ppm)	1.5(1)	2.2(1)	25.5(1.3)	16.1(8)	14.4(7)
Ga	1.20(6)	1.40(7)	1.90(10)	1.20(6)	0.80(4)
Zn	21.5(1.1)	8.9(4)	11.2(6)	8.2(4)	4.1(2)
V	128.8(6.4)	45.8(2.3)	19.2(1.0)	13.1(0.7)	5.1(0.3)
Mn	697(35)	465(23)	387(19)	310(16)	155(8)
Cd	0.6(0(3)	0.50(3)	0.40(2)	0.30(2)	0.10(1)
Pb	0.50(3)	0.20(1)	0.10(1)	0.10(1)	0.10(1)
Sn	0.10(1)	0.20(1)	0.10(1)	0.10(1)	0.10(1)
Nb	29.3(1.5)	11.7(6)	1.5(1)	1.0(1)	0.20(1)
W	15.4(8)	0.60(3)	0.10(1)	0.10(1)	0.20(1)
Metal					
Si	0.04(1)	3.20(6)	7.31(15)	10.27(21)	11.62(23)
Fe	94.5(1.9)	91.1(1.8)	84.0(1.7)	81.1(1.6)	78.1(1.6)
P	0.38(1)	0.63(1)	0.73(1)	0.89(2)	0.85(2)
Au	4.12(8)	3.24(6)	5.64(11)	5.53(11)	4.97(10)
Total	99.04	98.12	97.68	97.81	95.59
Ga (ppm)	39(2)	38(2)	58(3)	47(2)	81(4)
Zn	361(18)	534(27)	609(30)	702(35)	867(43)
V	42(2)	655(33)	486(24)	576(29)	215(11)
Mn	175(9)	2600(130)	4000(200)	4534(227)	2950(148)
Cd	28.0(1.4)	49.0(2.5)	86.0(4.3)	43.0(2.2)	28.0(1.4)
Pb	23.0(1.2)	27.0(1.4)	50.0(2.5)	18.0(9)	47.0(2.4)
Sn	9.4(5)	12.3(6)	21.5(1.1)	19.8(1.0)	17.4(9)
Nb	4.4(2)	166(8)	58(3)	148(7)	48(2)
W	12.3(6)	5.9(3)	2.4(1)	5.2(3)	3.4(2)
X(Fe)	0.98	0.91	0.83	0.77	0.75
X(FeO)	0.022	0.010	0.0012	0.0013	0.0005
ΔIW	−3.31	−3.90	−5.66	−5.53	−6.38
ln (1-XSi)	0.000	−0.066	−0.154	−0.216	−0.250
D(Au)	27500(3800)	14700(2000)	2210(300)	3440(480)	3450(480)
D(Fe)	31.5(4.4)	65.5(9.2)	494(69)	451(63)	1120(157)
D(Ga)	32.5(4.6)	27.1(3.8)	30.5(4.3)	39.2(5.5)	101.3(14.2)
D(Zn)	16.8(2.4)	60.0(8.4)	54.4(7.6)	85.6(12.0)	211.5(29.6)
D(V)	0.33(5)	14.3(2.0)	25.3(3.5)	44.0(6.2)	42.2(5.9)
D(Mn)	0.25(4)	5.6(8)	10.3(1.4)	14.6(2.0)	19.0(2.7)
D(Cd)	46.7(6.5)	98(14)	215(30)	143(20)	280(39)
D(Pb)	46(6)	134(19)	497(70)	182(25)	471(66)
D(Sn)	94(14)	62(9)	215(30)	198(28)	174(24)
D(Nb)	0.15(2)	14.2(2.0)	38.7(5.4)	148(21)	240(34)
D(W)	0.80(10)	9.8(1.4)	24.0(3.0)	52.0(7.0)	17.0(2.0)
ln Kd Au	7.72(1.08)	6.70(94)	3.73(52)	4.18(59)	3.67(51)
ln Kd Ga	−2.73(38)	−3.92(55)	−6.84(96)	−6.37(89)	−6.84(96)

Table 1 (*Continued*)

Experiment	2	3	5	6	7
ln Kd Zn	−1.54(25)	−0.969(16)	−3.12(50)	−2.55(41)	−2.61(42)
ln Kd V	−7.34(1.03)	−4.56(64)	−7.03(98)	−6.25(88)	−7.71(1.08)
ln Kd Mn	−5.74(86)	−3.28(49)	−4.71(71)	−4.25(64)	−4.95(74)
ln Kd Cd	−0.517(83)	−0.474(76)	−1.74(28)	−2.04(33)	−2.32(37)
ln Kd Pb	−0.523(73)	−0.169(24)	−0.904(13)	−1.79(25)	−1.81(25)
ln Kd Sn	−3.53(49)	−5.27(74)	−8.03(1.12)	−7.79(1.09)	−9.79(1.37)
ln Kd Nb	−11.8(1.7)	−8.89(1.24)	−12.9(1.8)	−11.1(1.6)	−13.0(1.8)
ln Kd W	−8.29(1.16)	−7.10(99)	−10.2(1.4)	−9.12(1.27)	−12.1(1.7)
ln Kd P	−14.47(2.02)	−16.28(2.28)	−25.68(3.60)	−23.85(3.34)	−28.38(3.97)

17.1 ± 3.8, and 23.1 ± 3.5, respectively, whereas P yielded the highest value of ε_M^{Si} at 55.0 ± 11.4 (Figs. 1, S-2).

Discussion

Comparison to low pressure epsilon parameters. Comparison of our newly determined 10 GPa ε_M^{Si} to values at 1 GPa (re-calculated to 2373 K using the following equation: $\varepsilon_i^{2373} = \varepsilon_i^{1873}\frac{1873}{2373}$) from previous studies) shows very similar values at both pressures (Fig. 1). Zn, V, Cd, and Nb are all shifted to higher values at 10 GPa, but the differences are within error. Similarly, Pb is slightly lower than the 1 GPa value, but still within error. Nb has the largest difference in measured epsilon values at low pressure and 10 GPa (albeit still within error), suggesting there might be a measurable pressure effect at even higher pressures. However, the low pressure value in Figure 1 was taken from the Steelmaking Data Sourcebook (1988) and is a value of −0.66, compared to our 10 GPa value of 7.0 ± 8.3. These experimental differences in the two studies are likely important and thus make difficult a comparison between low and high pressure values to assess a pressure effect. Despite these small differences for a few elements, our 10 GPa data are largely indistinguishable from the 1 GPa data and indicate that activity coefficients are not strongly dependent upon pressure.

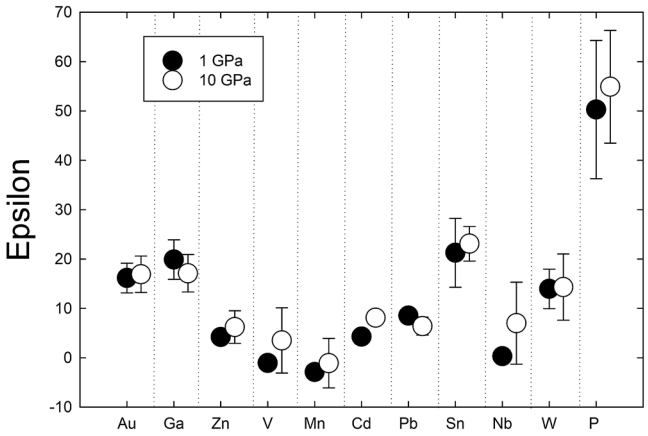

Figure 1 Comparison of 1 GPa and 10 GPa epsilon interaction parameters, with the 1 GPa values re-calculated from 1873 to 2373 K as discussed in the text. P, Au, Ga, Sn, Cd, Pb, Nb, W, Zn and V all have positive ε_M^{Si}, indicating that Si will cause a decrease in D metal/silicate with Si present in the metallic liquid. Mn has a negative ε_M^{Si}, indicating that Si will cause a very slight increase in D(Mn) metal/silicate with Si present in the metallic liquid. Nb exhibits the largest difference in measured in ε_M^{Si} at low pressure and 10 GPa, suggesting there might be a measurable pressure effect at even higher pressures.

Steenstra *et al.* (2020) examine the effect of pressure on ε_M^{Si} combining their data at 1 to 4 GPa with 11 GPa data from Vogel *et al.* (2018), for 12 elements, some of which we have examined here. Our results for Cd, Pb, Mn, V, and Sn are in overall agreement – none of these elements shows discernable change between 1 and 10 GPa. Steenstra *et al.* (2020) also present some evidence for change at high pressure for ε_M^{Si} for Ni, In, As and Sb, but change in those series occurs between 1 and 2 GPa and change above that is negligible (*i.e.*, 2 GPa = 11 GPa values for As, Sb, Sn). Pb, Cu, Cr, Mn, V, and Cd ε_M^{Si} all show no trend at higher pressures, similar to most elements we have examined here.

Implications. The accretion of terrestrial planets is a process that begins in the earliest Solar System as differentiated bodies form within a few million years after the start of the Solar System or T_0 (Kleine *et al.*, 2009; Levison *et al.*, 2015). The process continues with oligarchic growth of planetesimals (Kokubo and Ida, 1998) and then transitions to growth by merging and impact of planetesimals into planets (*e.g.*, Chambers, 2013). As this process unfolds, the energetics of accretion increase steadily providing sufficient energy to melt – either partially or completely – planetary mantles and metal-silicate mixtures (*e.g.*, de Vries *et al.*, 2016). The equilibration of metal and silicate melts is rapid and complete during this process (Kendall and Melosh, 2016; Lherm and Deguen, 2018) and thus the siderophile element content of the molten portion of the planet will change as the depth and associated pressure of metal-silicate equilibrium increases (*e.g.*, Rubie *et al.*, 2003). Modelling of siderophile element contents of molten upper mantle melts in equilibrium with Fe-Si-S-C metallic liquids during accretion now includes 26 elements (Fig. 2), including moderately siderophile and refractory (Ni, Co, Mo, and W), moderately siderophile and volatile (P, Ga, Cu, Ge, Sb, As, In, Bi, Sn, Ag, Cd, and Pb), weakly siderophile (Mn, Cr, V, Zn), and highly siderophile (Au, Pd, Pt, Re, Os, Ru) elements. The number of elements that can be modelled for Fe-Si-S-C liquids using this approach has nearly tripled since 2016.

A complete understanding of this large group of elements is desirable for a number of reasons. First, some of these elements are critical to biochemical processes and the origin of life, being part of energetically favourable enzymes or participants in chemical processes (*e.g.*, W, Mo, P, Ni, Co; Falkowski *et al.*, 2008; Kim *et al.*, 2013; Benner *et al.*, 2019), taking part in biochemical processes at black smokers, or involved in respiration (V, Cu, and Zn). For example, enhanced concentration of P in terrestrial or extrasolar planetary mantles is expected in equilibrium with Fe-Si liquids (Righter *et al.*, 2018). Higher concentrations in the mantle would aid the eventual transfer of P to the crust

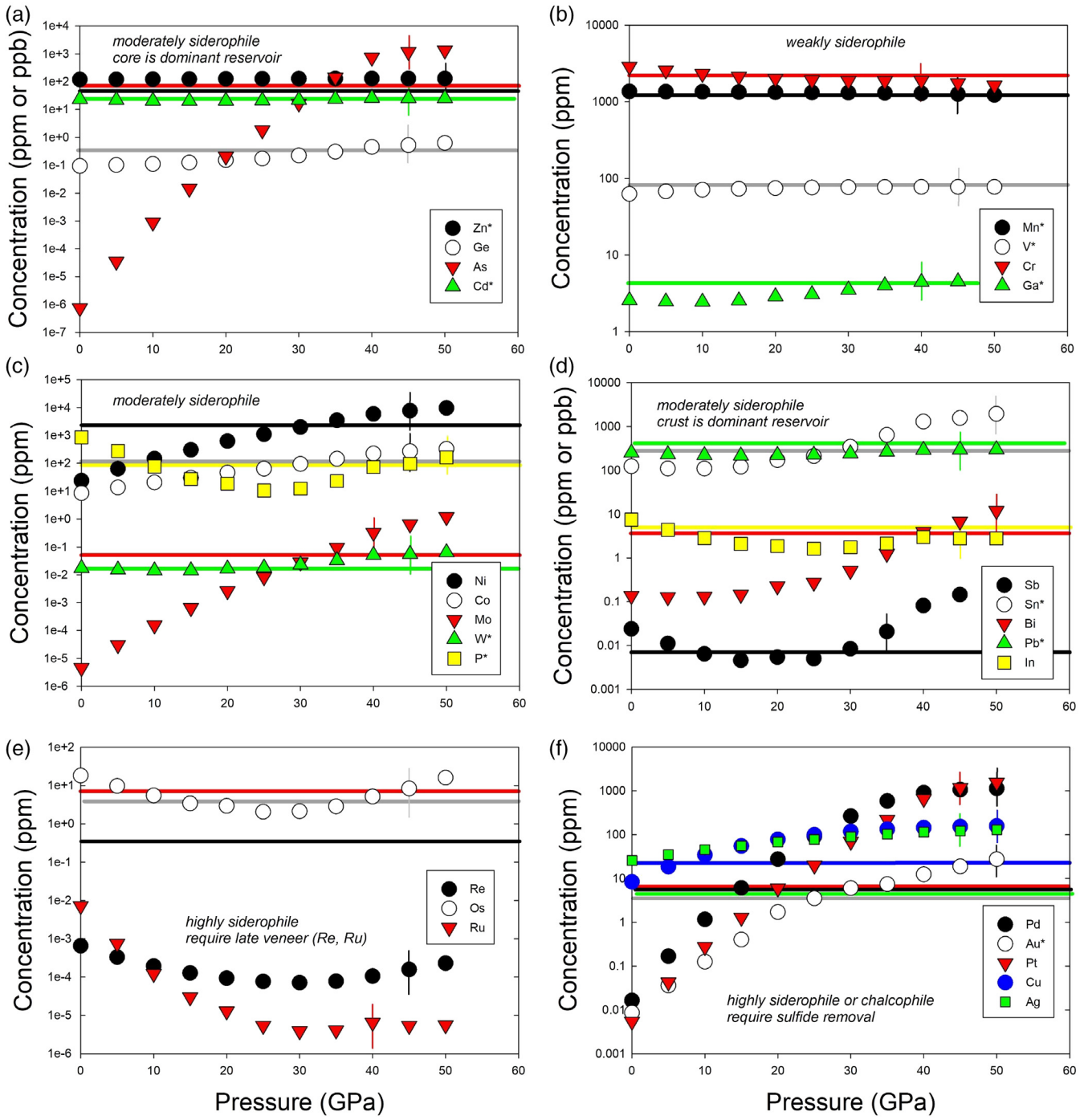

Figure 2 Evolution of siderophile element content of a terrestrial magma ocean as accretion proceeds and the PT conditions of metal-silicate equilibrium increase. Primitive upper mantle (PUM) siderophile element concentrations (from Palme and O'Neill, 2014) are horizontal lines with colour matching the symbols of the calculated values in each panel. The concentrations of 19 elements can be explained by metal-silicate equilibrium in a near 30–40 GPa magma ocean (Ni, Co, Mo, W, P, Mn, V, Cr, Ga, Zn, In, Ge, Sb, As, Sn, Bi, Cd, and Pb). Calculated concentrations of some elements such as Ag, Cu, Au, Pd, Pt become higher than PUM values, indicating the need for a removal mechanism such as a sulfide matte or late metallic segregation (see Righter *et al*. 2018, for detailed discussion). These 5 elements, together with Re, Os, and Ru, ultimately have their mantle concentrations set by addition of chondritic material after core formation and sulfide segregation.

(Supplementary Information Part 4), thus influencing the stability of P-bearing biochemicals such as ADP, RNA, and DNA in habitable planets. Second, the highly siderophile elements (*e.g.*, Au, Ru, Ir, Os), chalcophile elements (Cu, Ag), and volatile trace metals are frequently employed in constraining post core formation and late accretion processes (*e.g.*, Walker, 2009) as well as how Earth (and other bodies) acquired volatiles in general (*e.g.*, Halliday, 2013; Righter *et al.*, 2019). And third, the distribution of most siderophile elements between core, mantle and crust is dominated by the core, but the distribution of several exceptional elements is actually dominated by the crust (*e.g.*, Bi, Sn, As, Sb, Mo, W, Pb, In; Fig. 3). All of these elements exhibit positive ϵ_M^{Si} values, indicating their mantle concentrations would be elevated by equilibration with Fe-Si core-forming alloy. The higher mantle concentrations would also enhance the ultimate transfer of these elements to the crust and produce

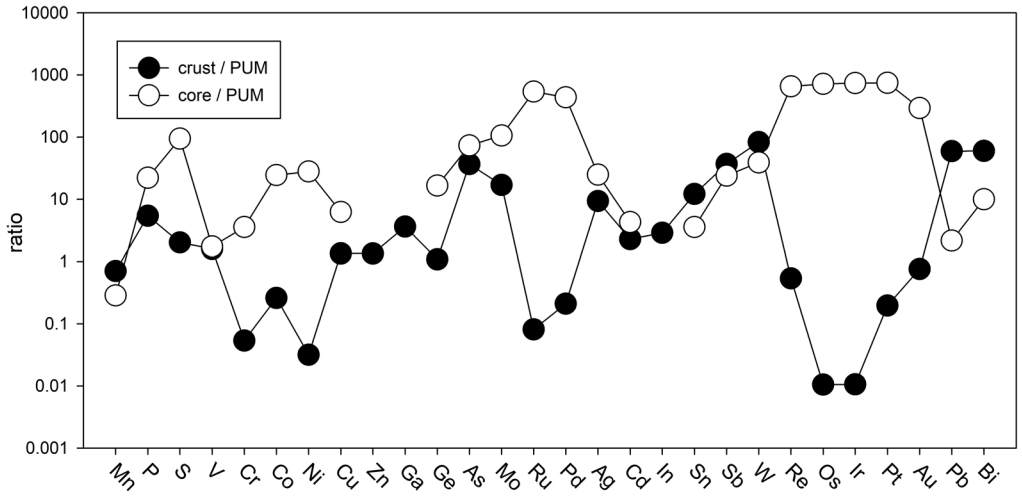

Figure 3 Concentrations of siderophile elements in the crust (Rudnick and Gao, 2014) and core (McDonough, 2003) of the Earth, normalised to values in the primitive upper mantle (PUM) (Palme and O'Neill, 2014). This diagram demonstrates that most siderophile elements are concentrated into the core, but there is an important and significant subset that is more highly concentrated into the crust, including Mn, Bi, Pb, In, Sn, Sb, and W.

similar or higher concentrations in the crust compared to the core (Fig. 3). Thus, a complete understanding of how all these siderophile elements became established in the primitive mantle and ultimately in the crust is essential to understanding the basic geochemistry of the early Earth.

The current work includes moderately siderophile and refractory (W), moderately siderophile and volatile (P, Cd, Sn, Pb), weakly siderophile (Mn, V, Ga, Zn, Nb), and highly siderophile (Au) elements. Most elements in these 4 groups exhibit no pressure effect on the activity coefficients in Fe-Si liquids, perhaps a surprising result because some have argued that structural changes in metallic liquids in this pressure range may lead to changes in partitioning behaviour in the Fe-C and Fe-Si liquids (5.2 GPa in Fe-C; Sanloup *et al.*, 2011, and 1-4 GPa in Fe-Si; Shibazaki *et al.* 2015). Although one might expect changes in epsilon parameters (and thus activity coefficients) due to such structural changes, our results suggest that there is no effect up to 10 GPa. It is possible that Fe-Si liquids do not undergo such structural changes below 10 GPa (*e.g.*, Sanloup *et al.*, 2004), and thus we do not see a change in activity coefficients. Some changes are proposed at higher pressures (*e.g.*, Morard *et al.*, 2007; Fe-S), and so detection of changes in activity coefficients at higher pressures should be pursued as well. In the meantime, because our results show no evidence for such structural changes in Fe-Si liquids below 10 GPa, the epsilon parameters can be employed in modelling equilibria at pressures up to 10 GPa.

Further studies of other siderophile elements at 10 GPa should be undertaken for comparison to the current results and to measure potential pressure effects on activity coefficients. Most elements should also be studied to pressures higher than 10 GPa and up to 70 GPa – pressures more applicable to those during the accretion of larger terrestrial planets. In particular, Cu, Mo, Bi, As, Sb, as well as the highly siderophile elements (HSE) Pt and Pd all exhibit pressure dependence, and thus pressure effects on activity coefficients must be thoroughly understood and studied in more detail. Additionally, a better understanding of the effect of pressure on Nb would be important to evaluating the Nb content of the mantle of differentiated bodies and the overall distribution cores and mantles in differentiated bodies (*e.g.*, Nebel *et al.*, 2010; Münker *et al.*, 2017).

Acknowledgements

This work was supported by NASA Planetary Science Division (MH), and an RTOP to KR from the NASA Cosmochemistry program.

Editor: Anat Shahar

Additional Information

Supplementary Information accompanies this letter at https://www.geochemicalperspectivesletters.org/article2034.

Cite this letter as: Righter, K., Rowland II, R., Yang, S., Humayun, M. (2020) Activity coefficients of siderophile elements in Fe-Si liquids at high pressure. *Geochem. Persp. Let.* 15, 44–49.

References

Armstrong, K., Frost, D.J., McCammon, C.A., Rubie, D.C., Ballaran, T.B. (2019) Deep magma ocean formation set the oxidation state of Earth's mantle. *Science* 365, 903–906.

Benner, S.A., Bell, E.A., Biondi, E., Brasser, R., Carell, T., Kim, H.-J., Mojzsis, S.J., Omran, A., Pasek, M.A., Trail, D. (2019) When Did Life Likely Emerge on Earth in an RNA-First Process? *ChemSystemsChem*, doi: 10.1002/syst.201900035.

Chambers, J.E. (2013) Late-stage planetary accretion including hit-and-run collisions and fragmentation. *Icarus* 224, 43–56.

de Vries, J., Nimmo, F., Melosh, H.J., Jacobson, S.A., Morbidelli, A., Rubie, D.C. (2016) Impact-induced melting during accretion of the Earth. *Progress in Earth and Planetary Science* 3, 7.

Falkowski, P.G., Fenchel, T., Delong, E.F. (2008) The microbial engines that drive Earth's biogeochemical cycles. *Science* 320, 1034–1039.

Halliday, A.N. (2013) The origins of volatiles in the terrestrial planets. *Geochimica et Cosmochimica Acta* 105, 146–171.

Hirose, K., Labrosse, S., Hernlund, J. (2013) Composition and state of the core. *Annual Review of Earth and Planetary Sciences* 41, 657–691.

Kendall, J.D., Melosh, H.J. (2016) Differentiated planetesimal impacts into a terrestrial magma ocean: Fate of the iron core. *Earth and Planetary Science Letters* 448, 24–33.

Kim J., Senn S., Harel A., Jelen B., Falkowski P. (2013) Discovering the electronic circuit diagram of life: structural relationships among transition metal binding sites in oxidoreductases. *Philosophical Transactions of the Royal Society B* 368, doi: 10.1098/rstb.2012.0257.

Kleine, T., Touboul, M., Bourdon, B., Nimmo, F., Mezger, K., Palme, H. (2009) Hf-W chronology of the accretion and early evolution of asteroids and terrestrial planets. *Geochimica et Cosmochimica Acta* 73, 5150–5188, doi: 10.1016/j.gca.2008.11.047.

Kokubo, E., Ida, S. (1998) Oligarchic growth of protoplanets. *Icarus* 131, 171–178.

Levison, H.F., Kretke, K.A., Walsh, K.J., Bottke, W.F. (2015) Growing the terrestrial planets from the gradual accumulation of sub-meter-sized objects. *Proceedings of the National Academy of Sciences* 112, 14,180–14,185, doi: 10.1073/pnas.1513364112

Lherm, V., Deguen, R. (2018) Small-Scale Metal/Silicate Equilibration During Core Formation: The Influence of Stretching Enhanced Diffusion on Mixing. *Journal of Geophysical Research: Solid Earth* 123, 10,496–10,516.

McDonough, W.F. (2003) Compositional model for the Earth's core. In: Holland, H.D., Turekian, K.K. (Eds.) *Treatise on Geochemistry, Volume 2.* Pergamon, Oxford, 547–568.

Morard, G., Sanloup, C., Fiquet, G., Mezouar, M., Rey, N., Poloni, R., Beck, P. (2007) Structure of eutectic Fe–FeS melts to pressures up to 17 GPa: implications for planetary cores. *Earth and Planetary Science Letters* 263, 128–139.

Münker, C., Fonseca, R.O., Schulz, T. (2017) Silicate Earth's missing niobium may have been sequestered into asteroidal cores. *Nature Geoscience* 10, 822–826.

Nebel, O., van Westrenen, W., Vroon, P.Z., Wille, M., Raith, M.M. (2010) Deep mantle storage of the Earth's missing niobium in late-stage residual melts from a magma ocean. *Geochimica et Cosmochimica Acta* 74, 4392–4404.

Palme, H., O'Neill, H.S.C. (2014) Cosmochemical estimates of mantle composition. In: Holland, H.D., Turekian, K.K. (Eds.) *Treatise on Geochemistry, Volume 3.* Second edition, Elsevier, Oxford, 1–39.

Righter, K. (2011) Prediction of metal-silicate partition coefficients for siderophile elements: An update and assessment of PT conditions for metal-silicate equilibrium during accretion of the Earth. *Earth and Planetary Science Letters* 304 158–167.

Righter, K. (2016) Metal-Silicate Partitioning of Siderophile Elements and Core-Mantle Segregation. *Deep Earth: Physics and Chemistry of the Lower Mantle and Core*, Geophysical Monograph 217, 161–174.

Righter, K., Pando, K., Humayun, M., Waeselmann, N., Yang, S., Boujibar, A., Danielson, L.R. (2018) Effect of silicon on activity coefficients of siderophile elements (Au, Pd, Pt, P, Ga, Cu, Zn, and Pb) in liquid Fe: Roles of core formation, late sulfide matte, and late veneer in shaping terrestrial mantle geochemistry. *Geochimica et Cosmochimica Acta* 232, 101–123.

Righter, K., Pando, K., Ross, D.K., Righter, M., Lapen, T.J. (2019) Effect of silicon on activity coefficients of Bi, Cd, Sn, and Ag in liquid Fe-Si, and implications for differentiation and core formation. *Meteoritics & Planetary Science* 54, 1379–1394.

Righter, K., Herd, C.D., Boujibar, A. (2020) Redox processes in early Earth accretion and in terrestrial bodies. *Elements: An International Magazine of Mineralogy, Geochemistry, and Petrology* 16, 161–166.

Rubie, D.C., Melosh, H.J., Reid, J.E., Liebske, C., Righter, K. (2003) Mechanisms of metal–silicate equilibration in the terrestrial magma ocean. *Earth and Planetary Science Letters* 205, 239–255.

Rudnick, R.L., Gao, S. (2014) Composition of the continental crust. In: Holland, H.D., Turekian, K.K. (Eds.) *Treatise on Geochemistry, Volume 4.* Second edition, Elsevier, Oxford, 1–51.

Sanloup, C., Fiquet, G., Gregoryanz, E., Morard, G., Mezouar, M. (2004) Effect of Si on liquid Fe compressibility: Implications for sound velocity in core materials. *Geophysical Research Letters* 31, L07604.

Sanloup, C., Van Westrenen, W., Dasgupta, R., Maynard-Casely, H., Perrillat, J.P. (2011) Compressibility change in iron-rich melt and implications for core formation models. *Earth and Planetary Science Letters* 306, 118–122.

Shibazaki, Y., Kono, Y., Fei, Y. (2015) Microscopic structural change in a liquid Fe-C alloy of ~5 GPa. *Geophysical Research Letters* 42, 5236–5242.

Siebert, J., Corgne, A., Ryerson, F.J. (2011) Systematics of metal-silicate partitioning for many siderophile elements applied to Earth's core formation. *Geochimica et Cosmochimica Acta* 75, 1451–1489.

Steenstra, E.S., Seegers, A.X., Putter, R., Berndt, J., Klemme, S., Matveev, S., Bullock, E.S., van Westrenen, W. (2020) Metal-silicate partitioning systematics of siderophile elements at reducing conditions: A new experimental database. *Icarus* 335, 113391.

Steelmaking Data Sourcebook (1988) The Japan Society for the Promotion of Science: The 19th Committee on Steelmaking. Gordon and Breach Science Publishers, Montreux.

Tuff, J., Wood, B.J., Wade, J. (2011) The effect of Si on metal-silicate partitioning of siderophile elements and implications for the conditions of core formation *Geochimica et Cosmochimica Acta* 75, 673–690.

Vogel, A.K., Jennings, E.S., Laurenz, V., Rubie, D.C., Frost, D.J. (2018) The dependence of metal-silicate partitioning of moderately volatile elements on oxygen fugacity and Si contents of Fe metal: Implications for their valence states in silicate liquids. *Geochimica et Cosmochimica Acta* 237, 275–293.

Wade, J., Wood, B.J. (2005) Core formation and the oxidation state of the Earth. *Earth and Planetary Science Letters* 236, 78–95.

Walker, R.J. (2009) Highly siderophile elements in the Earth, Moon and Mars: update and implications for planetary accretion and differentiation. *Chemie der Erde-Geochemistry* 69, 101–125.

Geochemical Perspectives Letters

Activity coefficients of siderophile elements in Fe-Si liquids at high pressure

K. Righter, R. Rowland, II, S. Yang, M. Humayun

Supplementary Information

The Supplementary Information includes:

- 1) Experimental and Analytical Techniques
- 2) Phase Equilibria and Equilibrium
- 3) Determination of Epsilon Interaction Parameters
- 4) Stability of Phosphides in Early Earth Mantle
- Figures S-1 to S-3
- Supplementary Information References

1) Experimental and Analytical Techniques

Starting materials were a mixture of natural Knippa basalt (Lewis *et al*., 1993) (70% by mass), Fe metal (25% by mass), and Au metal (5% by mass); this is the same mixture as those used in previous studies at 1 GPa (Righter *et al*., 2018). Gold has a very low solubility in silicate melts and if natural (ppm) levels in the metal were used, it would be undetectable in the silicate melt. Therefore, Au was added to these higher levels to make its concentrations higher and detectable in the silicate melts. We know from our previous studies that addition of ~5% Au makes the solubility levels high enough to be measured in the quenched silicate melts of the run products (*e.g.*, Righter *et al*., 2015, 2018).

Finally, silicon metal was added to the silicate and metal mixtures at increments of 2 wt% (2, 4, 6, 8, and 10% by weight), to ensure a wide range of Si alloyed in the final quenched metallic liquids.

Experiments were carried out using the 880-ton multi-anvil press in the Experimental Petrology Laboratory, in the Astromaterials Research and Exploration Science Division at NASA Johnson Space Center. To attain PT conditions of 10 GPa and 2373 K, we utilised a 10/5 assembly (available through COMPRES; Leinenweber *et al*., 2012) in a Walker-module (Walker *et al*., 1990). Pressure was calibrated for this assembly using three different transitions between 9 and 20 GPa: SiO_2 transitions at 9.4 GPa and 1873 K), the transition in $(Mg_{82}Fe_{18})_2SiO_4$ from olivine to wadsleyite at 13.4 GPa and 1673 K, and the transition in Mg_2SiO_4 from wadsleyite to ringwoodite at 20.0 GPa and 1873 K. The assembly utilises a pre-cast ceramic octahedral pressure medium, Re foil furnaces, pyrophyllite gaskets, and temperature is monitored with type C Re/W thermocouples (Righter *et al*., 2008). Uncertainty in temperature and pressure are ±15-20 K and ±0.5 GPa, respectively, based on temperature gradients no larger than 25 K; the emf of the thermocouple has not been pressure-corrected. Single crystal MgO capsules contained the metal and silicate mixtures, and once loaded into the assembly, were pressurised before heating to the run temperature. Thermocouple failure in some cases led to the need to heat by power curve which was established using the correlation between power and temperature from previous experiments. Experimental run durations at the desired temperature were between 1 and 5 min, required to approach equilibrium; shutting off power to the experiments ensured a rapid temperature drop and quenching of the run products.

Metals and quenched silicate glasses were analysed for major and minor elements with Electron Probe Microanalysis (EPMA) at NASA Johnson Space Center using a Cameca SX100 microprobe. Operating conditions for metals and silicates included 15 kV accelerating voltage and 30 nA sample current, and 15 kV accelerating voltage and 20 nA sample current, respectively. In addition, standardisation was done using various metal (Fe, Ni metal), glass (basalt), and mineral (diopside, rhodonite, rutile, potassium feldspar, apatite, olivine) standards. Some metals and glasses had coarse-grained quench texture, and thus a defocused electron beam of 20-30 μm diameter was used for analysis. In these cases, 30-50 analytical points were averaged to obtain a representative composition. Uncertainties in microprobe analyses are ~1% for Ti, Fe, Mn, Ca, and K, and 2% for Si, Al, Mg, Na, and P.

Some elements were present in quantities too low to be detectable using EMPA. Therefore, many trace elements (defined as being <100 ppm in concentration) were measured using a more sensitive analytical approach -

Laser Ablation Inductively Coupled Plasma Mass Spectrometry (LA-ICP-MS). Each sample was analysed by an ElectroScientific Instruments (ESI) New Wave™ UP193FX excimer (193 nm) laser ablation system coupled to a Thermo Element XR™ Inductively Coupled Plasma Mass Spectrometer (ICP-MS) at the Plasma Analytical Facility of the National High Magnetic Field Laboratory, Florida State University. Isotopes measured included ^{29}Si, ^{31}P, ^{51}V, ^{53}Cr, ^{55}Mn, ^{57}Fe, ^{66}Zn, ^{71}Ga, ^{93}Nb, ^{111}Cd, ^{120}Sn, ^{182}W, ^{197}Au, ^{208}Pb, following the analytical protocol of Yang *et al*. (2015). ^{57}Fe and ^{29}Si were used as internal standards for metal+sulfide and for silicates, respectively. Laser fluence was 2 GW/cm^2, and relevant isobaric interferences are discussed in Yang *et al*. (2015). Relative sensitivity factors were obtained using Hoba IVB (Walker *et al*., 2008), Filomena IIA (Wasson *et al*., 1989) and NIST SRM 1263a for siderophile elements (Humayun *et al*., 2007; Gaboardi and Humayun, 2009; Humayun, 2012) and NIST SRM 610 glass, USGS basaltic glasses BHVO-2G, BIR-1G, and BCR-2G for lithophile elements (Jochum *et al*., 2011). Spot sizes of 50 μm at 50 Hz for 10 seconds were used to measure both silicate and metal portions of the samples. The average of multiple analyses (2-5) was used to obtain the representative compositions for silicates and metals in each sample. In all samples, Au, P, V, Mn, Ga, Zn, Cd, Sn, W, Pb, and Nb were detectable in both metals and silicates and thus all 11 elements could be included in the investigation. The relative standard deviation (RSD) of ~5% is typical for elemental abundances in metal and silicate from each of the runs.

2) Phase Equilibria and Equilibrium

In all experiments, metallic liquid equilibrated with silicate melt, and the MgO capsule reacted with the silicate melt to form more MgO-rich liquids. The run products contain a mixture of glass and coarse-grained, skeletal-shaped, quench silicate crystals (Figure 1), because most of our liquids contain > 20% MgO, and MgO-rich silicate melts are generally difficult to quench to a glass even at high quench rates. Similarly, metallic liquids also quench to a matte of quench crystals, rather than a single phase. For analyses of our run products, metallic regions were selected from the largest metallic spheres, and closest to the silicate melt regions. Typically several large (50 μm) spots were measured on any given metallic sphere and then averaged to obtain a representative analysis. For silicate melts analyses, multiple 50 μm spots were identified and selected that were representative of the melt, and avoiding capsule MgO, small metallic blebs, or equilibrium growth oxides or silicates that might interfere with determination of a liquid composition. This approach has been discussed and reported in detail by (Righter *et al*., 2017).

Some studies of HSEs report the stability and existence of micronuggets of HSE-rich metal (*e.g.*, Ertel *et al*., 2008; Malavergne *et al*., 2016), and because Au is an HSE, and we have added a small amount of Au (5%) to the metallic portion of the experiment, this effect must be considered. However, we observed no HSE or Au micronuggets in our experiments (Fig. 1). Furthermore, if any HSE particles appeared as "spikes" in the analysis of the glasses, they could be filtered out during the data reduction, as also explained by (Righter *et al*., 2015).

In order to promote more reduced conditions in the experiments, elemental Si was added to the metal phase. Oxygen fugacity can be calculated relative to the iron-wüstite (IW) oxygen buffer, and we used the expression $\Delta IW = -2*\log [X_{Fe}/X_{FeO}]$, or otherwise referred to as "ΔIW". The ΔIW values for our experiments ranged from ~ -3.3 for low Si runs to ~ -6.4 for Si bearing runs (Table 1). ΔIW can also be calculated using activities of Fe and FeO instead of mole fractions, and thus the equation becomes $\Delta IW = -2*\log [a_{Fe}/a_{FeO}]$. For this calculation a_{Fe} in metal was calculated using the epsilon interaction parameter model for metallic liquids (*e.g.*, Righter *et al*., 2018), and a_{FeO} in silicate melt was calculated using the results of Holzheid *et al*. (1997). ΔIW values calculated using activities are slightly higher than those using mole fractions, from IW-2.9 to -6.11 (Table 1). Most studies utilise the mole fraction approach, and therefore we include those in the tables and figures. However, it is important to understand the difference in these two approaches that is caused by the non-ideality in the Fe-Si system. Activities are used in all the calculations of accretion and core-mantle equilibrium. The range of ΔIW values typically considered relevant to Earth's accretion and core formation is IW-4 to IW-2, and falling right in the middle of the range of relative fO_2 for these experiments. This relative fO_2 brack*et al*so produces a wide range of Si concentrations in the metal (and thus of ln $(1-X_{Si})$) that minimises error on the epsilon value.

3) Determination of Epsilon Interaction Parameters

Concentrations of Au, P, and other siderophile elements in metal and silicate (see Supplementary Information sections 1 and 2) were used to calculate Fe-M exchange K_d according to this equation (where M is the trace element of interest):

$$MO_{(n/2)}^{sil} + (n/2)Fe^{met} = M^{met} + (n/2)FeO^{sil} \quad \text{(Eq. S-1)}$$

Equation S-1 can be expanded to,

$$\ln K = \ln \frac{[a_M^{metal}][a_{FeO}^{silicate}]^{n/2}}{[a_{MO(n/2)}^{silicate}][a_{Fe}^{metal}]^{n/2}} = \ln \frac{[X_M^{metal}][X_{FeO}^{silicate}]^{n/2}}{[X_{MO(n/2)}^{silicate}][X_{Fe}^{metal}]^{n/2}} + \ln \frac{[\gamma_M^{metal}][\gamma_{FeO}^{silicate}]^{n/2}}{[\gamma_{MO(n/2)}^{silicate}][\gamma_{Fe}^{metal}]^{n/2}} \quad \text{(Eq. S-2)}$$

Then, setting $K_d = \frac{[X_M^{metal}][X_{FeO}^{silicate}]^{n/2}}{[X_{MO(n/2)}^{silicate}][X_{Fe}^{metal}]^{n/2}}$ and using the approach detailed by Wood *et al*., (2014), the ratio of oxide activity coefficients in the silicate, $\frac{[\gamma_{FeO}^{silicate}]^{n/2}}{[\gamma_{MO(n/2)}^{silicate}]}$, is assumed to be constant because the silicate melt compositions in this study are all similar. The metal composition, however, varies significantly in Si content and the ratio of activity coefficients in the metal, $\frac{[\gamma_M^{metal}]}{[\gamma_{Fe}^{metal}]^{n/2}}$, is dependent upon variation in metal composition. The above equations are re-arranged yielding:

$$\ln K_d = \text{constant} + n/2 \ln \gamma_{Fe}^{metal} - \ln \gamma_M^{metal} \quad \text{(Eq. S-3)}$$

Equation S-3 is then combined with $\ln \gamma_M^{metal} = \ln \gamma_{Fe}^{metal} + \ln \gamma_M^0 - \varepsilon_M^{Si} \ln(1-X_{Si})$ to become:

$$\ln K_d - (n/2 - 1) \ln \gamma_{Fe}^{metal} = \text{const} - \ln \gamma_M^0 + \varepsilon_M^{Si} \ln(1-X_{Si}) \quad \text{(Eq. S-4)}$$

In Equation S-4, γ_M^0 is defined as the activity coefficient of M at infinite dilution, γ_{Fe}^{metal} is defined as the activity coefficient of Fe in Fe metal (*e.g.*, as in Righter *et al*., 2017, 2018), and ε_M^{Si} is an interaction parameter (*e.g.*, Lupis, 1983) that is a measure of the effect of a solute such as Si (in Fe metallic liquid) on the activity of a trace element that liquid (*e.g.*, As, Sb, Ge, or In; Righter *et al*., 2017). The slope of $\ln K_d$ versus $\ln(1-X_{Si})$ in Equation S-4 provides ε_M^{Si} directly for each element at 2373 K and 10 GPa.

The interaction parameter ε_M^{Si} can be used to calculate activity coefficients (γ) for a trace metal (i) in a multi-component (N) system according to:

$$\begin{aligned} \ln \gamma_i = {} & \ln \gamma_{Fe} + \ln \gamma_i^0 - \varepsilon_i^j \ln(1 - X_i) \\ & - \sum_{j=1(j\neq i)}^{N-1} \varepsilon_i^j X_j \left(1 + \frac{\ln(1 - X_j)}{X_j} - \frac{1}{1 - X}\right) \\ & + \sum_{j=1(j\neq i)}^{N-1} \varepsilon_i^j X_j^2 X_i \left(\frac{1}{1 - X_i} + \frac{1}{1 - X_j} + \frac{X_i}{2(1 - X_i)^2} - 1\right) \end{aligned}$$

Where X_i, X_j and γ_i, γ_j are mole fractions and activity coefficients of components i and j, respectively, and γ_i^0 is the activity of i in Fe at infinite dilution (from Ma, 2001; Righter *et al*., 2017). We calculated interaction parameter ε_M^{Si} for Au, P, V, Mn, Ga, Zn, Cd, Sn, W, Pb, and Nb, by using a linear fit to the data, with the standard error (1 sigma) and the fits passing variance tests in SigmaPlot 12.0.

4) Stability of Phosphides in Early Earth Mantle

Phosphorus can be stable in phosphates and phosphides, with the latter being more soluble than the former. Some have argued that phosphates are stable to secondary alteration processes in the crust, thus locking up P and requiring an extraterrestrial late accreted source (Pasek, 2008). However, P prefers more soluble phosphides at early terrestrial mantle oxygen fugacities of IW-2, based on the equilibrium:

$$2P + 3CaSiO_3 + 5/2O_2 = Ca_3(PO4)_2 + 3SiO_2 \qquad \text{(Eq. S-5)}$$

and thermodynamic data from Robie *et al*. (1978) (Fig. S-3). Phosphides may thus facilitate transfer of P to the crust by secondary alteration processes in the early Earth.

Supplementary Figures

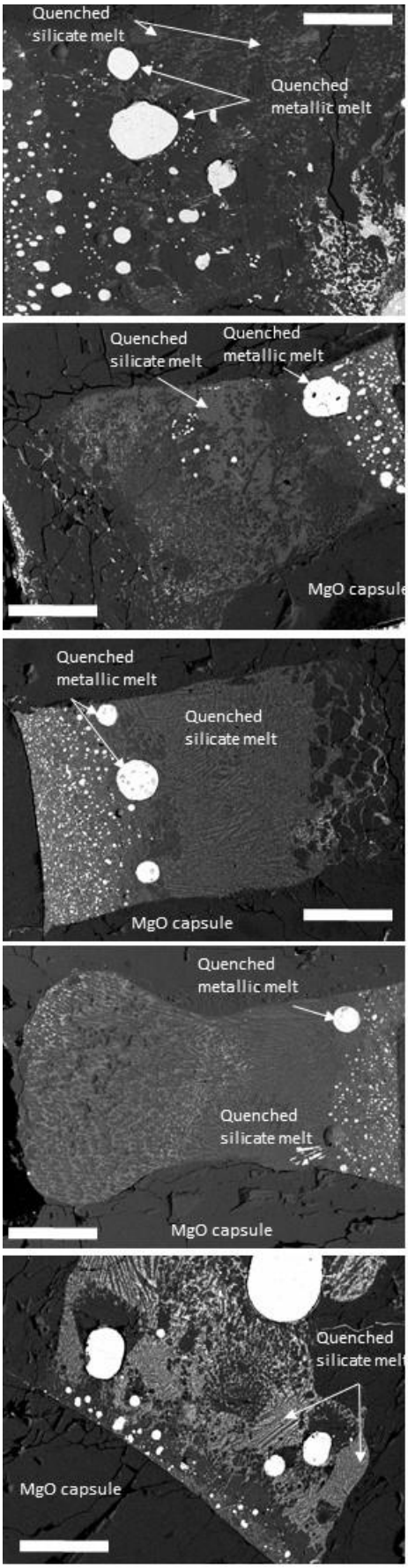

Figure S-1 BSE images of Experiments 2, 3, 5, 6, and 7. For each experiment, images show the bright white metallic liquid, and lighter gray silicate melts which mostly quenched to a matte of quench crystals. All experiments were carried out in MgO capsules, which reacted slightly with the silicate melt. All scale bars are 200 μm.

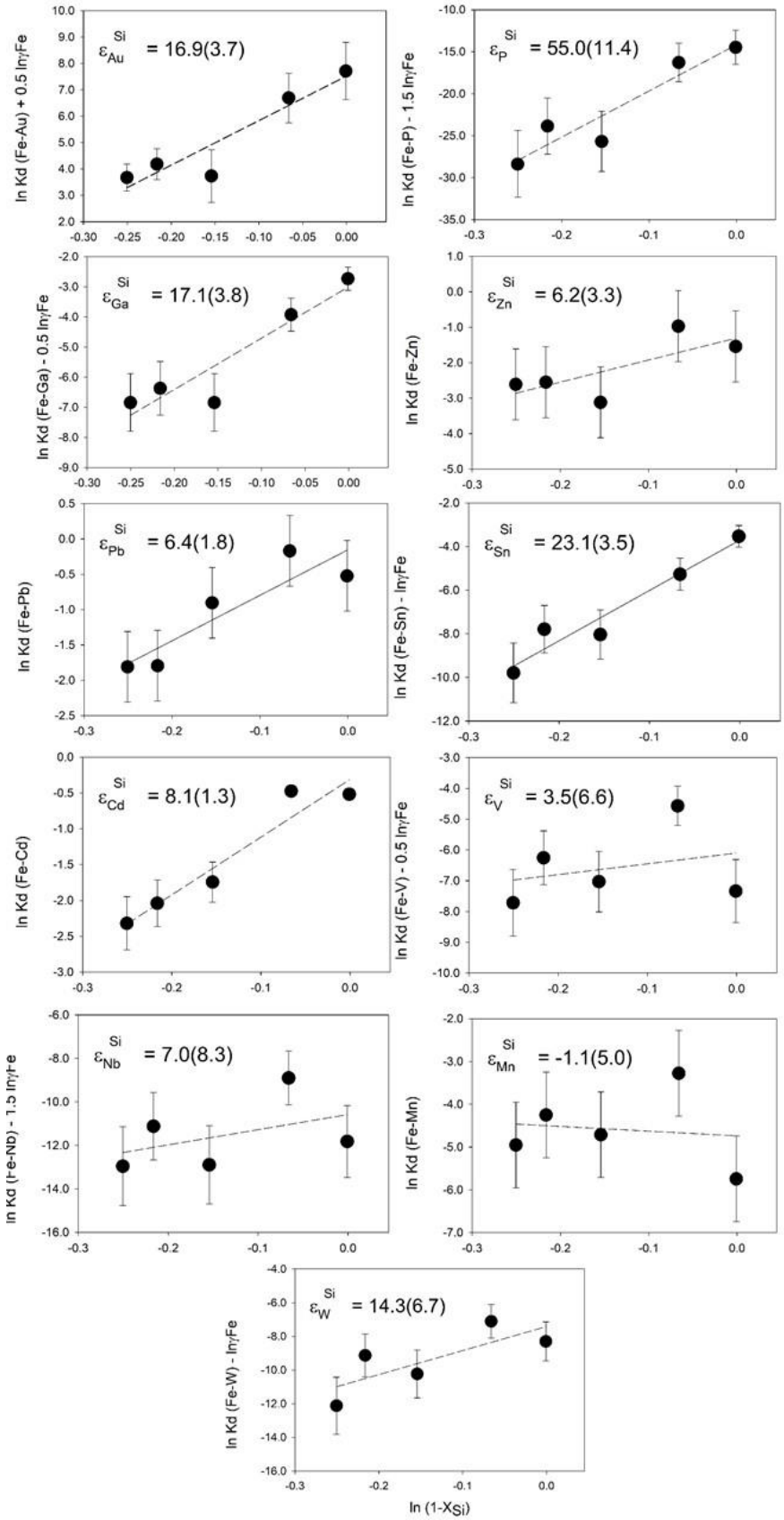

Figure S-2 ln K_d versus ln (1-Xsi) for all elements measured in this study. lnK_d(Fe-X^{5+})–1.5ln(γ_{Fe}), ln K_d(Fe-X^{4+})–ln(γ_{Fe}), ln K_d(Fe-X^{3+})–0.5ln(γ_{Fe}), ln K_d(Fe-X^{2+}), and ln K_d(Fe-X^{1+})+0.5ln(γ_{Fe}) versus ln(1-X_{Si}) from experiments across a wide range of Si contents in metallic Fe. The slope of the lines yields the interaction parameter for each – ε_X, - in Fe-Si liquids.

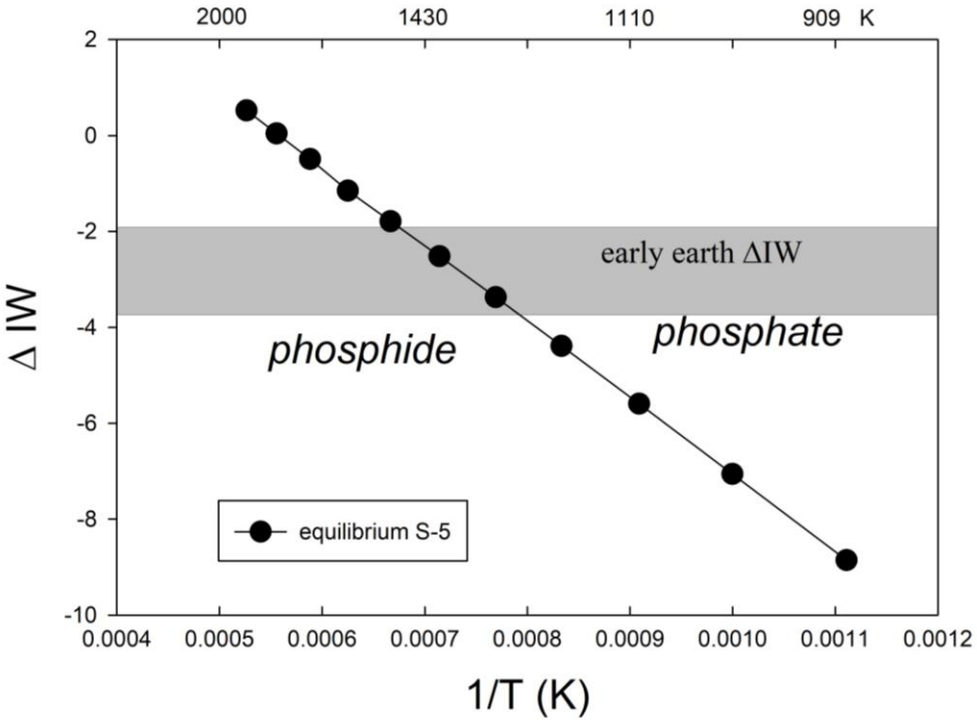

Figure S-3 Oxygen fugacity relative to the iron-wüstite buffer (IW) calculated form thermodynamic data from Robie *et al*. (1978) for equilibrium (Eq. S-5). IW reference buffer is calculated using the expression of Campbell *et al*. (2009). Note that phosphide is stable at high temperatures and fO_2 of the early Earth. Calculations assume $aSiO_2 = aCaSiO_3 = aCa_3(PO_4)_2 = 1$, and aP = 0.01.

Supplementary Information References

Campbell, A.J., Danielson, L., Righter, K., Seagle, C.T., Wang, Y., Prakapenka, V.B. (2009) High pressure effects on the iron–iron oxide and nickel–nickel oxide oxygen fugacity buffers. *Earth and Planetary Science Letters* 286, 556-564.

Ertel, W., Dingwell, D.B., Sylvester, P. (2008) Siderophile elements in silicate melts—A review of the mechanically assisted equilibration technique and the nanonugget issue. *Chemical Geology* 248, 119-139.

Gaboardi, M., Humayun, M. (2009) Elemental fractionation during LA-ICP-MS analysis of silicate glasses: Implications for matrix-independent standardization. *Journal of Analytical Atomic Spectrometry* 24, 1188-1197.

Holzheid, A., Palme, H., Chakraborty, S. (1997) The activities of NiO, CoO and FeO in silicate melts. *Chemical Geology* 139, 21-38.

Humayun, M., Simon, S.B., Grossman, L. (2007) Tungsten and hafnium distribution in calcium–aluminum inclusions (CAIs) from Allende and Efremovka. *Geochimica et Cosmochimica Acta* 71, 4609-4627.

Humayun, M. (2012) Chondrule cooling rates inferred from diffusive profiles in metal lumps from the Acfer 097 CR2 chondrite. *Meteoritics & Planetary Science* 47, 1191-1208.

Jochum, K.P., Weis, U., Stoll, B., Kuzmin, D., Yang, Q., Raczek, I., Günther, D. (2011) Determination of reference values for NIST SRM 610–617 glasses following ISO guidelines. *Geostandards and Geoanalytical Research* 35, 397-429.

Leinenweber, K.D., Tyburczy, J.A., Sharp, T.G., Soignard, E., Diedrich, T., Petuskey, W.B., Wang, Y., Mosenfelder, J.L. (2012) Cell assemblies for reproducible multi-anvil experiments (the COMPRES assemblies). *American Mineralogist* 97, 353–368.

Lewis, R.D., Lofgren, G.E., Franzen, H.F., Windom, K.E. (1993) The effect of Na vapor on the Na content of chondrules. *Meteoritics* 28, 622–628.

Lupis, C.H. (1983) Chemical Thermodynamics of Materials. Elsevier Science Publishing Co., Inc., New York, NY., 581 pp.

Ma, Z. (2001) Thermodynamic description for concentrated metallic solutions using interaction parameters. *Metallurgical and Materials Transactions B* 32, 87-103.

Malavergne, V., Charon, E., Jones, J., Cordier, P., Righter, K., Deldicque, D., Hennet, L. (2016) The formation of nuggets of highly siderophile elements in quenched silicate melts at high temperatures: Before or during the silicate quench? *Earth and Planetary Science Letters* 434, 197-207.

Pasek, M.A. (2008) Rethinking early Earth phosphorus geochemistry. *Proceedings of the National Academy of Sciences* 105, 853-858.

Righter, K., Humayun, M., Danielson, L. (2008) Partitioning of palladium at high pressures and temperatures during core formation. *Nature Geoscience* 1, 321-323.

Righter, K., Danielson, L.R., Pando, K., Williams, J., Humayun, M., Hervig, R.L., Sharp, T.G. (2015) Mantle HSE abundances in Mars due to core formation at high pressure and temperature. *Meteoritics & Planetary Science* 50, 604-631.

Righter, K., Nickodem, K., Pando, K., Danielson, L., Boujibar, A., Righter, M., Lapen, T.J. (2017) Distribution of Sb, As, Ge, and In between metal and silicate during accretion and core formation in the Earth. *Geochimica et Cosmochimica Acta* 198, 1-16.

Righter, K., Pando, K., Humayun, M., Waeselmann, N., Yang, S., Boujibar, A., Danielson, L.R. (2018) Effect of silicon on activity coefficients of siderophile elements (Au, Pd, Pt, P, Ga, Cu, Zn, and Pb) in liquid Fe: Roles of core formation, late sulfide matte, and late veneer in shaping terrestrial mantle geochemistry. *Geochimica et Cosmochimica Acta* 232, 101-123.

Robie, R.A., Hemingway, B.S., Fisher, J.R. (1978) Thermodynamic properties of minerals and related substances at 298.15 K and 1 Bar (10^5 Pascals) pressure and at higher temperatures. *United States Geological Survey Bulletin* 1452, Washington DC, 461 pp.

Walker, D., Carpenter, M.A., Hitch, C.M. (1990) Some simplifications to multianvil devices for high pressure experiments. *American Mineralogist* 75, 1020-1028.

Walker, R.J., McDonough, W.F., Honesto, J., Chabot, N.L., McCoy, T.J., Ash, R.D., Bellucci, J.J. (2008) Modeling fractional crystallization of group IVB iron meteorites. *Geochimica et Cosmochimica Acta* 72, 2198-2216.

Wasson, J.T., Ouyang, X., Wang, J., Jerde, E. (1989) Chemical classification of iron meteorites: XI. Multi-element studies of 38 new irons and the high abundance of ungrouped irons from Antarctica. *Geochimica et Cosmochimica Acta* 53, 735-744.

Wood, B.J., Kiseeva, E.S., Mirolo, F.J. (2014) Accretion and core formation: The effects of sulfur on metal–silicate partition coefficients. *Geochimica et Cosmochimica Acta* 145, 248-267.

Yang, S., Humayun, M., Righter, K., Jefferson, G., Fields, D., Irving, A.J. (2015) Siderophile and chalcophile element abundances in shergottites: Implications for Martian core formation. *Meteoritics & Planetary Science* 50, 691-714.